Atmospheric General Circulation Model Simulations With an Interactive Ocean: Effects of Sea Surface Temperature Anomalies in the Arabian Sea

Leonard M. Druyan[1]
Institute for Space Studies, Goddard Space Flight Center, NASA
New York N.Y. and
Department of Geography, Bar Ilan University, Ramat Gan, Israel[2]

James R. Miller
Department of Meteorology and Physical Oceanography
Rutgers University, New Brunswick, New Jersey

and

Gary L. Russell
Institute for Space Studies, Goddard Space Flight Center, NASA
New York, N.Y.

[Original manuscript received 27 August 1981; in revised form 15 October 1982]

ABSTRACT *Three different simulations using an atmospheric general circulation model (GCM) with a 65-m deep interactive ocean have been analysed for a 4-month period (April–July) in the Arabian Sea area. Although the ocean model contains no dynamics, it accounts indirectly for the transport of heat due to dynamic processes such as upwelling and horizontal advection. The first simulation does not include ocean heat transport, and the SST increases too much during the 4-month period. The second simulation includes oceanic heat transport, and the final SST field is within a few per cent of the climatological SST field. The ocean transports are obtained by assuming that they are the differences between the vertical heat fluxes across the air-sea interface as calculated from the GCM and the change in heat content of a 65-m deep interactive ocean. The third simulation incorporates an initial negative SST anomaly into the ocean model with transport and analyses the effect of this anomaly on the ocean and the atmosphere. The effects on the ocean arise because of feedback from the atmosphere. In the ocean, the northern part of the SST anomaly propagates from the western boundary downwind*

[1]Senior Resident Research Associate at NASA under the sponsorship of the National Research Council/ National Academy of Science.

[2]On sabbatical leave during the 1979–1980 academic year.

ATMOSPHERE-OCEAN 21 (1) 1983, 94–106 0705-5900/83/0000-0094$01.25/0

across the Arabian Sea while the southern part of the anomaly disappears. This occurs primarily because of changes in the latent heat fluxes. In the atmosphere, an increase in precipitation to the east of the initial anomaly propagates downwind ahead of the propagating SST anomaly until it eventually appears over India in July.

RÉSUMÉ *On analyse trois simulations différentes s'étendant sur une période de quatre mois chacune (avril à juillet) dans la mer d'Arabie en utilisant un modèle de la circulation générale atmosphérique (MCG) ayant un océan interdépendant profond de 65 m. Quoique le modèle à océan ne contienne pas de dynamique, il parvient à expliquer indirectment le transport de chaleur résultant de processus dynamiques tels que la résurgence et l'advection horizontale. Au cours de la première simulation, où l'océan n'est pas représenté, le transport de chaleur ainsi que la température de la mer en surface (TMS) augmentent rapidement au cours d'une période de quatre mois. Dans la deuxième simulation qui contient le transport de chaleur océanique, la TMS est à quelques pourcents près du champ climatologique de cette dernière. On calcule les transports océaniques en posant comme hypothèse qu'ils sont donnés par les différences entre le flux vertical de chaleur à l'interface air-mer, tels que calculés par le MCG, et le changement du contenu en chaleur de l'océan interdépendant profond de 65 m. La troisième simulation incorpore au modèle à océan et à transport une anomalie négative dans le champ de la TMS et analyse l'effet de cette anomalie sur l'océan ainsi que l'atmosphère. Les effets sur l'océan sont causés par les rétroactions de l'atmosphère.*

Dans la mer, on trouve que le secteur nord de l'anomalie de la TMS se propage avec le vent à partir de la lisière ouest vers la mer d'Arabie, tandis qu'elle disparaît dans le secteur sud. Ceci se produit à cause des changements dans les flux de la chaleur latente principalement. Dans l'atmosphère, un accroissement de la précipitation à l'est de l'anomalie originale se propage dans le sens du vent et en avant de l'anomalie en propagation jusqu'à ce qu'il apparaît éventuellement aux Indes en juillet.

1 Introduction

Many authors have suggested that observed sea-surface temperature anomalies (SSTA) act as stimuli for subsequent atmospheric behaviour (Bjerknes, 1972; Namias, 1978). General circulation models (GCM) have been applied to test various hypotheses regarding the influence of SSTA on the atmospheric flow, but rarely do their numerical results support the theories proposed in the observational studies (Spar and Atlas, 1975; Spar et al., 1976; Washington et al., 1977).

Because of their economic, social and political importance, the characteristics of summer monsoon rains over India have been a popular subject of studies dealing with the effect of sea-surface temperature on the evolution of weather systems. Shukla and Misra (1977) showed that Arabian Sea surface temperatures and local rain over India were correlated, although not to the extent of demonstrating a predictive relationship. Using the GCM of the Geophysical Fluid Dynamics Laboratory, Shukla (1975, 1976) found that the imposition of SSTA of 0 to -3°C in the western Arabian Sea caused a significant reduction in summer monsoon rainfall over India, while Washington et al. (1977) and Druyan (1982b) found the same SSTA produced statistically significant reductions only locally over water. In each case a different GCM was used, although only in the third did the model climatology show the observed large seasonal increases in rainfall over India associated with the summer monsoon. This model is also used in the present study. In this experiment, however, an attempt is made to account for the modification of the initial SSTA due to atmospheric influences.

Ramage (1977) suggested that SSTA are established by atmospheric forcing and are likely to be more influenced by atmospheric evolution than to change the course of this evolution. He concluded, therefore, that the relevance of much of the testing with GCMs is limited because there is no opportunity for realistic feedback; SST anomalies are imposed and remain insensitive to the atmospheric evolution. A GCM that incorporates some measure of ocean-atmosphere interaction is therefore advantageous.

This study describes a scheme whereby SST, used as the lower boundary for ocean areas in a GCM developed at the Goddard Institute for Space Studies, is treated as a predicted variable, without benefit of a fully interactive, dynamic ocean model. Accordingly, the SST is made sensitive to evolving changes in the overlying atmosphere. The analysis of the time change of SST at selected locations illustrates an application of the scheme and signals encouragement for pursuing refinements in future work. We have applied this GCM to trace the evolution of SSTA in the western Arabian Sea and have examined the impact of SSTA on Indian summer monsoon rainfall by comparing results from a parallel control simulation using the same model.

2 Description of the model

The simulations discussed here have been obtained with an atmospheric general circulation model in conjunction with three different ocean models. The atmospheric model, Model I described by Hansen et al. (1983), is a three-dimensional climate model with $8° \times 10°$ horizontal resolution and seven vertical layers. Integration of the dynamic equations is accomplished using Arakawa's scheme B. The source terms include a comprehensive radiation scheme and parameterizations of condensation and surface interaction. The model incorporates realistic topography and land-ocean coverage. Druyan (1982a) has shown that the model does simulate the evolution of the summer monsoon circulation and precipitation over southern Asia.

Three different ocean models are considered. The first uses climatologically specified (CS) ocean temperatures and ice coverage as given by Washington and Thiel (1970). Druyan (1982a) has discussed the GCM simulation of the monsoon when climatological SST fields are used. The second model assumes a uniformly mixed 65-m deep ocean with no ocean transport (NOT); SST, and the thickness and horizontal extent of ice are predicted. The third ocean model is similar to the second but includes ocean transport (OT).

The ocean transports of heat are obtained as follows. Twenty-four hour integrals of vertical energy fluxes between the atmosphere and the ocean and ocean ice are saved from a one-year run of the CS model. This vertical flux includes solar and thermal radiation, sensible heat, latent heat and precipitation heat (including negative energy for snow). For each water grid point of the atmospheric model, the temporal variation of vertical flux is fitted by least squares to its first harmonic as

$$VF(t) = A \cos \omega t + B \sin \omega t + C \tag{1}$$

where A, B and C are the fitted parameters in units of W m^{-2}, ω is 2π/year, and t is time.

The heat in the ocean is assumed to be stored in the upper 65 m of water, and the CS

model updates its climatological ocean temperatures and ice thicknesses daily. The temporal variation of that heat content is fitted by least squares to its first harmonic as

$$HC(t) = D \cos \omega t + E \sin \omega t + F \tag{2}$$

where D, E and F are in units of J m^{-2}.

The ocean transport necessary to approximately maintain the climatological equilibrium of the CS model at each water grid point is

$$OT(t) = \frac{\partial HC}{\partial t} - VF = (\omega E - A) \cos \omega t + (-\omega D - B) \sin \omega t - C \tag{3}$$

When the OT model uses this transport, its simulation of the annual cycle of ocean temperatures is generally within a fifth of a degree of the climatological values of the CS model on a monthly latitudinal average. The models are not as accurate near the summer pole, since the OT model has to choose between melting the ice or warming the ocean. The NOT model on the other hand, becomes several degrees too warm in the tropics after a few months. (See Fig. 1.)

Although we will use (3) to determine the transport of heat within the ocean, it must be noted that this term also includes errors in the GCM's vertical energy flux and errors caused by assuming that all heat in the ocean is stored in the upper 65 m. An ensemble of runs has not been completed with the OT model, and therefore the noise level of the model is not known. Miller et al. (1982) have shown that annual values of ocean heat transport computed from this model are in agreement with those in other studies.

3 Model simulations

Three different 4-month model simulations starting with April 1 initial conditions will be discussed. The first simulation is performed with the NOT model starting with April 1 climatological ocean temperatures. Since this model does not yield the actual climatological SST field at the end of the 4-month simulation, the OT model discussed in Section 2 is introduced. Starting with the same ocean temperatures as the NOT model, the OT model produces a temperature field at the end of the 4-month period that agrees well with climatology. The third simulation shows the effects of introducing an SST anomaly in the ocean transport model (OTA).

Figure 1 shows the comparison of SST changes for the three simulations for eleven model grid boxes in the western Arabian Sea. Each of these grid boxes is assumed to be all-ocean in the model, and the three curves in each box show the SST variations for that grid box for each of the three simulations, NOT, OT and OTA. It should be noted again that the introduction of transport in the model does not represent an attempt to parameterize the ocean dynamics but simply represents an attempt to include the effects of the climatological dynamics (both upwelling and horizontal advection) on local heat balance.

Figure 1 shows that the SST increases too much in the NOT simulation. South of 10°N the climatological SST decreases during the 4-month period, but in the NOT simulation the SST actually increases by several degrees. The increase occurs

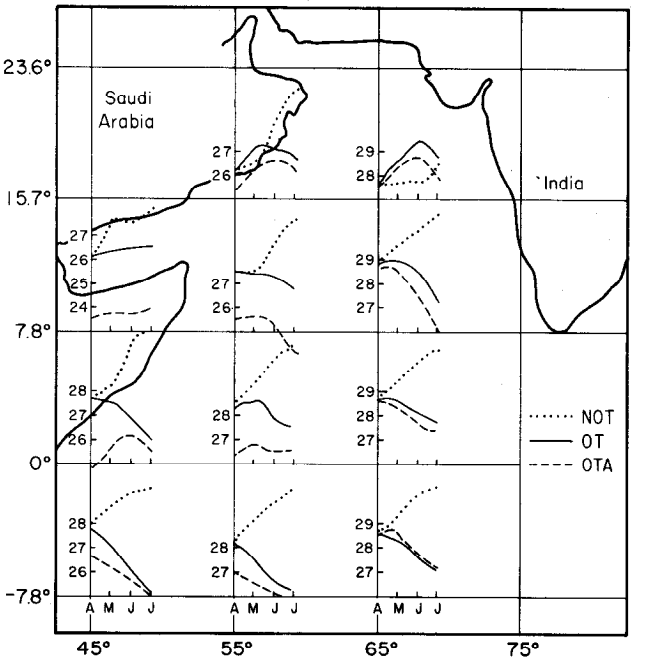

Fig. 1 Sea-surface temperature changes for the April–July period for the three different simulations. The dotted, solid and dashed curves are for the NOT, OT and OTA runs, respectively. Grid box boundaries are delineated by the latitude and longitude lines.

because of the increased absorption of heat during this period. At the end of the period the temperature difference between the runs with and without transport can be almost 5°C at some locations in the western part of the basin.

Much of the large temperature increase in the NOT simulation may be due to the choice of a 65-m interactive ocean. The work of Düing (1970) indicates that the monsoonal influence extends downward to 200 m in the eastern part of the basin and to more than 300 m in the western part. If the surface heat fluxes were distributed over a deeper layer, the temperature increase in the NOT simulation would be considerably less. However, the major difference between the simulations with and without transport would remain – the SST increases when transport is not included and mostly decreases when transport is included. Near the western boundary the temperature decrease in the OT simulation is due primarily to upwelling and horizontal advection. The cooling in the western Arabian Sea between April and June, with the greatest cooling along the coast, has been discussed by Düing and Schott (1978) and Düing and Leetma (1980). In the following subsection the OT simulation will be considered as the control run, and the effect of an SST anomaly on the ocean and atmosphere in the western Arabian Sea will be studied.

a *Anomaly Simulation (Oceanic Effects)*

In this subsection we compare the results of the OT simulation, which is initialized with April climatological SSTs, and the OTA simulation, which is initialized with an

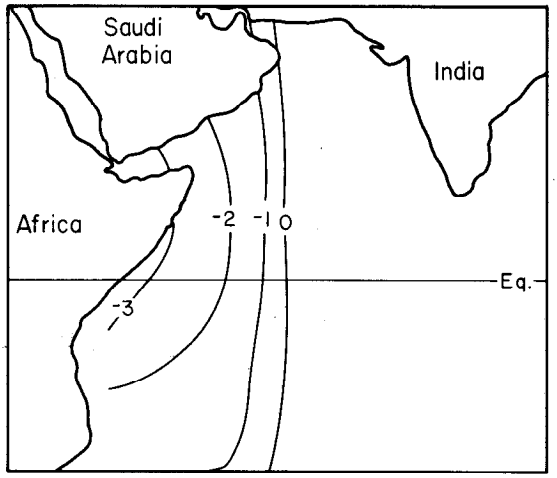

Fig. 2 Initial SST anomaly field (°C) imposed in the OTA simulation.

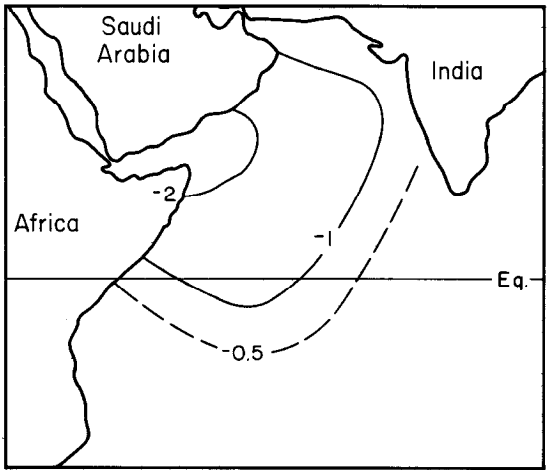

Fig. 3 SST anomaly (°C) at the end of the four-month OTA simulation.

anomaly in the climatological SST field. Figures 2 and 3 show the initial anomaly field on April 1 and the SST anomaly field at the end of the 4-month OTA simulation, respectively. Since the OT model generates a July SST field in good agreement with the July SST climatology, Fig. 3 also shows the difference between the SST fields generated by the OTA and OT simulations. Since the OT simulation allows the ocean temperature to respond to atmospheric stimuli, it is particularly interesting to monitor the evolution of the initial SST anomaly in the OTA simulation.

Figure 3 shows that the northern part of the original anomaly is still present at the end of the OTA simulation. During the same period, most of the southern part of the original anomaly has disappeared. The initial anomaly has also elongated along an east-west axis indicating the development of a new negative departure over the

TABLE 1. Monthly mean heat budget components (W m^{-2}) computed for the grid box centred at 4°N, 50°E. Vertical flux quantities are positive downward. Ocean transport and net energy fluxes are positive into the grid box.

	Latent Heat Flux		Sensible Heat Flux		Net Radiative Flux		Ocean Transport		Net Energy Flux	
Month	OT	OTA	OT	OTA	OT	OTA	OT	OTA	OT	OTA
April	−110	−50	0	0	+210	+210	−90	−90	+10	+70
May	−145	−30	0	0	+205	+210	−110	−110	−50	+70
June	−135	−70	0	0	+195	+200	−125	−125	−65	+5
July	−110	−110	−10	0	+190	+200	−125	−125	−55	−35

TABLE 2. Same as Table 1, but for 12°N, 50°E.

	Latent Heat Flux		Sensible Heat Flux		Net Radiative Flux		Ocean Transport		Net Energy Flux	
Month	OT	OTA	OT	OTA	OT	OTA	OT	OTA	OT	OTA
April	−110	−140	−10	−10	+180	+190	−10	−10	+50	+30
May	−130	−150	−10	−15	+190	+195	−30	−30	+20	0
June	−140	−110	0	0	+190	+210	−50	−50	0	+50
July	−140	−90	0	−5	+190	+185	−65	−65	−15	+25

eastern Arabian Sea, downwind of the initial anomaly. In summary, the simulation suggests dissipation of the southern part of the cold anomaly because of negative feedback and propagation of the northern part of the anomaly downwind. The convergence of the SST curves in the southwest is due to a reduced cooling rate relative to the control run and even a reversal to warming in one case. The propagation of the SST anomaly downwind is due to increased cooling rates that are triggered by effects of the initial anomaly.

Heat budgets were calculated at each grid box to determine the reasons for the observed time changes of the SST field in the OTA simulation. Any net transfer of energy into a grid box increases the SST and vice versa. Since ocean transport of thermal energy was the same for OT and OTA, any differences in SST changes between them must be due to differences in the fluxes of latent heat, sensible heat and/or radiation at the air-sea interface. Of these, the latent heat flux was the most important. The convergence of the SST curves at the grid boxes shown in the southern portion of Fig. 1 indicates that the SSTs at those locations were nearly the same at the end of the OT and OTA simulations. Since the OTA simulation started with a lower SST than the OT simulation, there must have been correspondingly less cooling in the OTA simulation. Heat budget calculations show that there was a significant reduction in evaporation in this area, the most pronounced effect occurring at 4°N, 50°E where the mean upward latent heat fluxes of the OTA simulation were less than 52% of the OT values in April, May and June. Table 1 shows the monthly mean values of the heat budget components for this grid point.

In contrast to the southern region, the maintenance of the original SST departure in the northern region is due to continued high evaporation rates. Table 2 presents the heat budget for 12°N, 50°E, and shows that evaporative cooling was even enhanced

TABLE 3. Same as Table 1, but for 12°N, 70°E

	Latent Heat Flux		Sensible Heat Flux		Net Radiative Flux		Ocean Transport		Net Energy Flux	
Month	OT	OTA	OT	OTA	OT	OTA	OT	OTA	OT	OTA
April	−140	−170	−10	−10	+220	+210	−25	−25	+45	+5
May	−150	−195	−5	−10	+215	+225	−90	−90	−30	−70
June	−130	−170	0	−10	+225	+220	−130	−130	−35	−90
July	−140	−140	0	−10	+230	+210	−160	−160	−70	−100

relative to the control during April and May despite the 3°C lower SST. The reduction of the latent heat flux in June caused the SST to increase slightly and reduced the negative departure to only 2.3°C by the end of July.

The propagation of the original SST anomaly eastward in the northern region can be due to either a faster cooling or a slower warming in the OTA simulation. Figure 1 shows a faster cooling at 12°N, 70°E and a slower warming than in the control at 20°N, 70°E. Table 3 shows the heat budget components for each month at 12°N, 70°E. During the period from April to June, the evaporation has increased relative to the control and is principally responsible for the formation of the new SST anomaly. The negative departure continues through July owing to a reduction in solar radiation presumably because of more daytime cloudiness.

It has been shown that the differential evolution of the SST has been largely determined by changes in the latent heat fluxes, which constitute a large part of the local heat budget. The atmospheric model computes this flux from the expression

$$LH = L\rho KV(q_A - q_s), \tag{4}$$

where L is the latent heat of evaporation, ρ is air density, K is a transfer coefficient, V is the surface wind speed, q_A is the specific humidity of the air and q_s is the saturation specific humidity corresponding to the SST. Lowering the SST lowers q_s, so that if no other changes occur, the upward latent heat flux decreases. If, in addition, V should also decrease, evaporation is further reduced. This combination apparently occurred at 4°N, 50°E where the resultant surface wind speed for each of the four months was reduced by 1 m s^{-1} in the OTA simulation. Enhanced evaporation at 12°N, 70°E can be explained by increases in V since the resultant surface wind speed was slightly higher in April and May and 1–2 m s^{-1} higher in June.

Evaporation rates at 12°N, 50°E were higher during April and May in the OTA simulation even when the 3°C negative SST anomaly was introduced. Although the resultant wind speed was not increased, it is possible that higher wind speeds did enhance the evaporation during certain time steps. The enhanced evaporation is more likely due to a decrease of 4 g kg^{-1} in the monthly mean of q_A in the OTA simulation during April and May – i.e. drier air encourages greater evaporation. The wind directions in both cases, although 10–20° apart, were from the southwest, indicating advection of continental air into the grid box. In the adjacent grid box to the south, however, this reduction in specific humidity did not occur despite the lower SST, and the evaporation there was much less. At this location, resultant surface wind di-

rections were 90 and 140° for April and May, respectively, indicating the advection of humid maritime air.

Our discussion has neglected reference to the parameter K in (4), which is itself dependent on the air-sea temperature difference. Evaporation is increased when low static stabilities allow for vertical mixing, but can be completely stifled in extremely stable stratifications. Since K fluctuates considerably with time of day, evaporation must also undergo a diurnal cycle. Since only monthly means of the computed variables are available, it is difficult to determine the extent to which higher wind speeds caused the enhancement of evaporation.

b *Anomaly Simulation (Atmospheric Effects)*

The general pressure pattern over the north Indian Ocean during the summer monsoon derives from the northward-directed temperature gradient. Imposition of anomalously cold water should tend to intensify that gradient, at least in the lowest atmospheric layers, and this would influence, in turn, pressure gradients and wind speeds. Shukla (1975) examined the effect of the same cold SST anomaly specified in this study on overlying sea-level pressures in another atmospheric model and found increases of less than 1 mb. The important consequence of any such pressure increase is, however, its effect on wind speeds. Figure 4 shows the difference between the OTA and OT simulations of the magnitude of the surface wind vector over the area of the north Indian Ocean for June. The band of increased maximum wind speed extends eastward from the northeast side of the anomaly. The pattern of higher surface wind speeds over the north Arabian Sea and lower values over the south was less organized during April when the summer temperature gradient was weaker.

Figure 5 shows the difference between the mean evaporation rates (OTA − OT) in June over the north Indian Ocean. Comparison with Fig. 4 confirms that areas of enhancement coincide with areas of increased surface wind speed. Elsewhere, however, reductions in evaporation are apparently not due to decreases in the surface wind speed.

The impact of SSTA on monsoon rainfall rates was tested previously by Shukla (1975, 1976), Washington et al. (1977) and Druyan (1982b). In all of these experiments, however, the SST anomaly was held constant throughout the integration, and other SSTs were prescribed by climatology. In the OTA study, the initially imposed anomaly evolved with time in response to atmospheric changes. It has been shown above that the intensity and shape of the anomaly changed during the 4-month simulation; it is interesting to examine what impact this had on simulated precipitation rates within the monsoon system.

Figure 6 shows the differences between the OTA and OT simulations of May precipitation rates. Large reductions in rainfall occur along the eastern side of the cold SST anomaly, while small increases are located farther east and north. We cannot show statistical significance for any of the "impacts" because the variability of the OT version of the model has not been determined by an ensemble of parallel simulations from arbitrarily different initial conditions (see Chervin and Schneider, 1976). The pattern is, however, similar to that of the impacts obtained for the version of the model reported by Druyan (1982b).

Figure 7 shows the impact on July mean precipitation rates. Decreases are evident

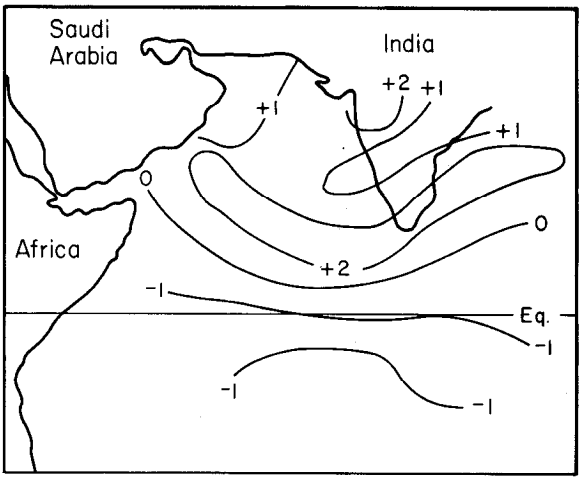

Fig. 4 Difference (m s^{-1}) between OTA and OT simulations of wind speed for June. Positive values indicate that the wind speed has increased in the OTA simulation.

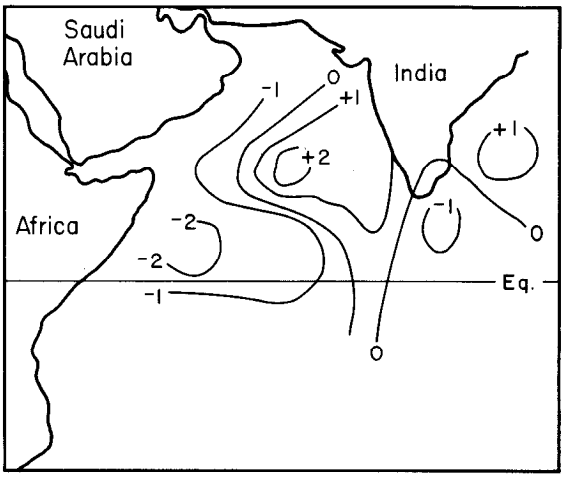

Fig. 5 Difference between evaporation rates (mm day^{-1}) in June, (OTA − OT).

over the entire Arabian Sea, consistent with the increase in stability created by the differential cooling of SST. *Increases* in the precipitation rates show up for the first time in the July means over India directly downwind of the anomalously cold water. Perhaps this enhancement of rainfall has reached the Indian continent because the cold SST anomaly spread eastward. When the SST anomaly patterns of Figs 2 and 3 are compared with the rainfall anomaly patterns of Figs 6 and 7, we note that the negative rainfall anomalies are located at the eastern edges of the cold anomalies. Farther east there are positive anomalies, and comparison of the above four figures indicates that the rainfall anomaly pattern moves eastward in conjunction with the eastward movement of the SST anomaly.

Washington et al. (1977) showed compensating convection downwind of their cold

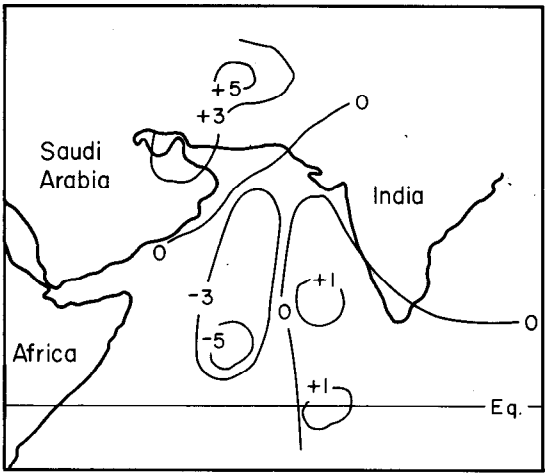

Fig. 6 Difference between the OTA and OT simulations (OTA − OT) of May precipitation rates (mm day^{-1}).

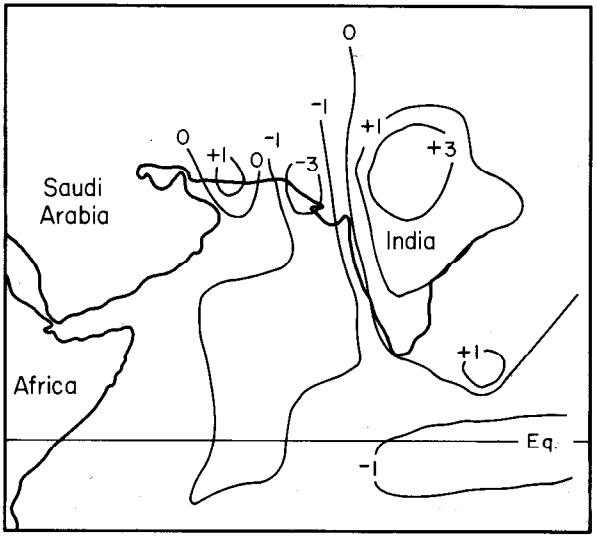

Fig. 7 As Fig. 6, except for July.

SST anomaly; Druyan (1982b) assumed that the air downwind of the cold water contained greater amounts of precipitable water as a result of reductions in precipitation over the stable, cold water region. (These generally exceed the reductions in evaporation.) The high humidity air then unloads the extra amounts of water vapour at the first opportunity for convection, in this case, over the hot continent.

Shukla's (1975) simulation with a similar but unchanging SSTA was made with the GFDL model. In contrast to the present results as well as those of Washington et al. (1977) and Druyan (1982b), he found reduced rainfall over India, presumably caused by the cold SST anomaly in the Arabian Sea. The different results here

undoubtedly derive from the use of different GCMs (with different climatologies) and different experimental designs. While we have shown the effect of an interactive anomaly over a four-month period, the former study considered only one simulated month, beginning in June. Beyond that month the reported effect is significantly reduced.

4 Summary

The principal results of this study were obtained by comparing three different simulations using an atmospheric GCM in conjunction with a 65-m deep interactive ocean. In the simulation without transport, (NOT), the SST increased during the 4-month period because of a net input of heat into the upper ocean. The increase in SST with this model was too large, possibly due to the choice of an interactive ocean that was too shallow. A second simulation, which incorporated ocean transport (OT) by assuming that the transport was the residual of the net heat fluxes and the change in heat content over the upper 65 m of ocean, was then used to simulate the climatological change of SST during the 4-month period. Although there were no ocean dynamics in this model, it was used to analyse some of the atmospheric and oceanic feedbacks that could arise if an initial anomaly was imposed on the SST field.

The third simulation (OTA) showed how an initial SST anomaly affected the atmospheric flow and precipitation patterns, and in turn how the atmospheric changes altered the initial SST anomaly. The initial negative SST anomaly was imposed along the western Arabian Sea with a maximum departure of -3°C at 10°N. The southern part of the anomaly disappeared by the end of the simulation, but in the northern section the anomaly moved in the direction of the wind toward the northeast across the ocean basin. Since the ocean transports in the control and the anomaly runs were the same, the northeastward movement of the anomaly was not due to ocean transport, and was therefore a response to a change in atmospheric parameters. In the northern region, the increase in the latent heat flux downwind of the anomaly, relative to the control, was partially due to an increase in wind speed. In the southern region, the evaporation was reduced, partially because of a decrease in the wind speed. The reduced rate of heat loss in the anomaly run caused the SSTs of the anomaly and control runs to converge. Hence, SST anomalies may be propagated by the atmospheric flow through feedbacks between the atmosphere and ocean. If more realistic ocean dynamics were incorporated, different feedbacks could be expected.

The propagation and subsequent development of the SSTA were discussed, and its effect on the atmospheric precipitation field was also analysed. Since an ensemble of such simulations was not made, the statistical significance could not be determined. The precipitation pattern, however, showed that in May there were large reductions in the precipitation rates along the eastern side of the cold anomaly and small increases farther east and north, but no effects over India. By July, however, the SST anomaly had propagated downwind, the corresponding precipitation pattern had shifted as well, and an increase in precipitation occurred over India. It would be of considerable interest to obtain additional simulations using an ocean model containing realistic dynamics, to determine the effect on the various feedbacks discussed in this paper.

References

BJERKNES, J. 1972. Large-scale atmospheric response to the 1964–65 Pacific equatorial warming. *J. Phys. Oceanogr.* **2**: 212–217.

CHERVIN, R. and S. SCHNEIDER. 1976. On determining the statistical significance of climate experiments with general circulation models. *J. Atmos. Sci.* **33**: 405–412.

DRUYAN, L. 1982a. Studies of the Indian summer monsoon with a coarse-mesh general circulation model. Part 1. *J. Climatol.* (in press).

———. 1982b. Ibid. Part 2.

DÜING, W. 1970. *The Monsoon Regime of the Currents in the Indian Ocean.* Int. Indian Ocean Exped. Oceanogr. Monogr. No. 1, East/West Center Press, Honolulu, 68 pp.

——— and F. SCHOTT. 1978. Measurements in the source region of the Somali current during the monsoon reversal. *J. Phys. Oceanogr.* **8**: 278–289.

——— and A. LEETMA. 1980. Arabian Sea cooling: A preliminary heat budget. *J. Phys. Oceanogr.* **10**: 307–312.

HANSEN, J.; G. RUSSELL, D. RIND, P. STONE, A. LACIS, S. LEBEDEFF, R. REUDY and L. TRAVIS. 1983. Efficient three-dimensional global model for climate studies: Models I and II. *Mon. Weather Rev.* (in press).

MILLER, J.; G. RUSSELL and L. TSANG. 1982. Annual oceanic heat transports computed from an atmospheric model. *Dyn. Atmos. Oceans* (in press).

NAMAIS, J. 1978. Multiple causes of the North American abnormal winter 1976–77, *Mon. Weather Rev.* **106**: 279–295.

RAMAGE, C. 1977. Sea-surface temperatures and local weather. *Mon. Weather Rev.* **105**: 540–544.

SHUKLA, J. 1975. Effects of Arabian Sea-surface temperature anomaly on Indian summer monsoon: A numerical experiment with the GFDL model. *J. Atmos. Sci.* **32**: 503–511.

———. 1976. Reply to Comments on the article by Shukla (1975). *J. Atmos. Sci.* **33**: 2253–2255.

——— and B.M. MISRA. 1977. Relationships between sea surface temperature and wind speed over the central Arabian Sea, and monsoon rainfall over India. *Mon. Weather Rev.* **105**: 998–1002.

SPAR, J. and R. ATLAS. 1975. Atmospheric response to variations in sea-surface temperatures. *J. Appl. Meteorol.* **14**: 1235–1245.

———; ——— and E. KUO. 1976. Monthly mean forecast experiments with the GISS model. *Mon. Weather Rev.* **104**: 1215–1241.

WASHINGTON, W. and L. THIEL. 1970. Digitized global monthly mean ocean surface temperatures. NCAR Tech. Note TN-54, Natl Cent. Atmos. Res., Boulder, Colo., 30 pp.

———; R. CHERVIN and G. RAO. 1977. Effects of a variety of Indian Ocean surface temperature anomaly patterns on the summer monsoon circulation: Experiments with the NCAR GCM. *Pure Appl. Geophys.* **115**: 1335–1356. Also in *Monsoon Dynamics*, T. Krishnamurti, Ed., Birkhauser Verlag.